

Un-mixing Test-time Adaptation under Heterogeneous Data Streams

Zixian Su*, Jingwei Guo*, Xi Yang†, Qiufeng Wang, Kaizhu Huang†

Abstract—Deploying deep models in real-world scenarios remains challenging due to significant performance drops under distribution shifts between training and deployment environments. Test-Time Adaptation (TTA) has recently emerged as a promising solution, enabling on-the-fly model adaptation. However, its effectiveness deteriorates in the presence of mixed distribution shifts – common in practical settings – where multiple target domains coexist. In this paper, we study TTA under mixed distribution shifts and move beyond conventional whole-batch adaptation paradigms. By revisiting distribution shifts from a spectral perspective, we find that the heterogeneity across latent domains is often pronounced in Fourier space. In particular, high-frequency components encode domain-specific variations, which facilitates clearer separation of samples from different distributions. Motivated by this observation, we propose to un-mix heterogeneous data streams using high-frequency domain cues, making diverse shift patterns more tractable. To this end, we propose Frequency-based Decentralized Adaptation (FreDA), a novel framework that decomposes globally heterogeneous data stream into locally homogeneous clusters in the Fourier space. It leverages decentralized learning and augmentation strategies to robustly adapt under mixed domain shifts. Extensive experiments across various environments (corrupted, natural, and medical) show the superiority of our method over the state-of-the-arts.

Index Terms—Test-time Adaptation, Transfer Learning

I. INTRODUCTION

DEEP learning models often suffer significant performance degradation when deployed in environments where the data distribution differs from that of the training set – a challenge known as domain shift [1], [2]. Recently, Test-Time Adaptation (TTA) [3]–[10] has emerged as a promising solution by refining model parameters to better align with the encountered data at inference time. It leverages the incoming data stream for real-time adjustments without the need for retraining on a labeled dataset, enabling swift model adaptation to unpredictable data characteristics during deployment.

Despite their success, current TTA models are often limited to ideal testing conditions, typically involving homogeneous test samples with similar types of distribution shifts. In reality, distribution shifts are *mixed*, *overlapping*, and *even conflicting* [11]–[14]. For instance, photo management software handles diverse corruptions, such as noise, blur, compression; medical imaging platforms manage inconsistencies from varied acquisition methods; and autonomous driving systems face fluctuating conditions like lighting, weather, and road types.

Zixian Su is with Beijing Academy of Artificial Intelligence, Beijing, China (E-mail: zxsu@baai.ac.cn); Jingwei Guo is with Alibaba Group, Beijing, China (E-mail: jingweiguol9@outlook.com); Xi Yang and Qiufeng Wang are with Xi’an Jiaotong-Liverpool University, Suzhou, Jiangsu, China (Email: xi.yang01@xjtlu.edu.cn; qiufeng.wang@xjtlu.edu.cn); Kaizhu Huang is with Duke Kunshan University, Kunshan, Jiangsu, China (Email: kaizhu.huang@dukekunshan.edu.cn).

*Equal contribution.

†Corresponding authors.

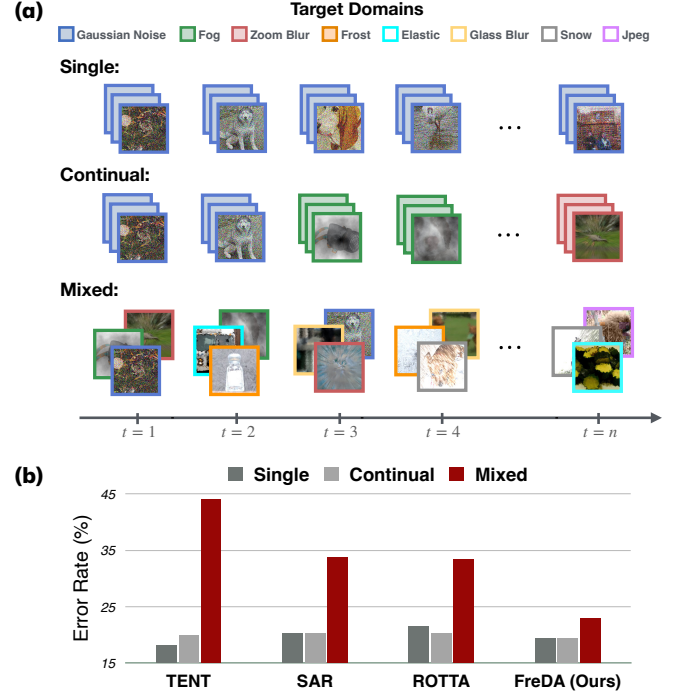


Fig. 1: (a) Illustration of different online distribution shifts, ranging from single-domain to continual and mixed-domain shifts, with increasing complexity and realism. (b) Classification error rate on CIFAR-10-C: while conventional models experience a sharp performance drop as distribution shifts become more complex, our method maintains superior performance, particularly under mixed-domain shifts.

Such complexity poses serious challenges for existing methods. While recent efforts have extended TTA to continually changing environments [5], they typically assume a uniform target domain at each time step, as illustrated in the continual setting in Fig. 1 (a). Some methods periodically reset the model to its source pre-trained state [7], [9] to mitigate the cumulative effect of sequential distribution shifts on adaptation. Others down-weight outlier target samples [6], [10] to suppress the impact of abrupt or rare shifts. Although these strategies aim to improve robustness under dynamic conditions, they lack the capacity to disentangle or localize domain variations within a batch. As a result, they often misalign conflicting domain shifts, failing to be deployed in realistic, heterogeneous data streams (see Fig. 1 (b)).

To address this, we propose shifting from coarse, homogeneous / whole-batch adaptation to a fine-grained strategy that explicitly disentangles heterogeneous shifts. Our approach leverages the spectral information to disentangle domain variations, which naturally separates sample features across fre-

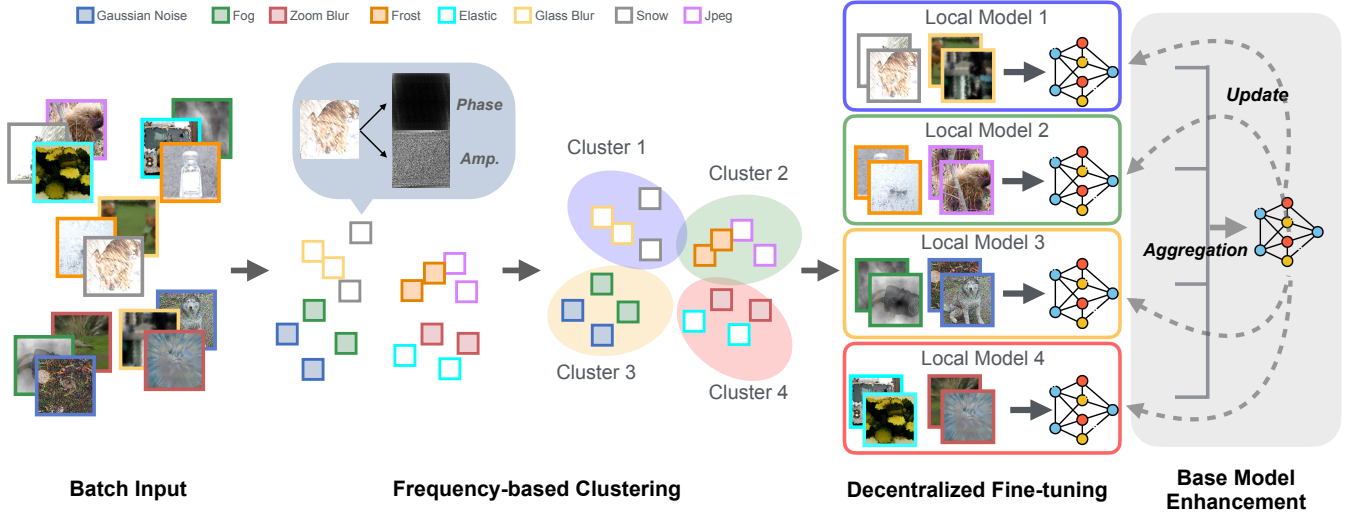


Fig. 2: Illustration of FreDA framework. Heterogeneous data streams are partitioned in Fourier space into locally homogeneous clusters, where local models adapt independently and synchronize weights for intermittent update.

quency bands: high-frequency components capture fine details like edges and textures, while low-frequency components represent global structures such as shape and illumination (see Section IV). By decomposing inputs accordingly, we are able to better characterize distributional variations and identify diverse shifts. Moreover, the Fourier transform operates directly on raw pixel-level inputs, independent of any pre-trained model, making it robust to large domain gaps and enhancing adaptability in real-world deployments.

Building upon this insight, we introduce Frequency-based Decentralized Adaptation (FreDA). FreDA begins by partitioning incoming data in the Fourier space, leveraging high-frequency components to group samples with similar domain characteristics. This transforms globally heterogeneous inputs into locally homogeneous subsets before any adaptation takes place. Multiple local models are then deployed, each assigned to a specific cluster, and adapt independently to their respective data streams while periodically uploading their parameters. These intermittent updates help build more stable model weights, reducing potential errors during clustering. To further enhance robustness, we introduce a Fourier-based augmentation scheme that improves sample quality and reinforces adaptation to shift-specific patterns. To summarize, the main contributions of this work are three-fold:

- We identify a key limitation of most existing TTA methods – their neglect of real-world data heterogeneity – which leads to suboptimal performance when confronted with diverse, mixed distribution shifts.
- We propose FreDA, a frequency-based decentralized adaptation framework that leverages spectral decomposition and localized adaptation to effectively address heterogeneous distribution shifts at test-time.
- We validate FreDA through extensive experiments on corrupted, natural, and medical benchmarks, demonstrating consistent improvements over state-of-the-art methods across various distribution shift scenarios.

II. CONNECTIONS TO PREVIOUS STUDIES

A. Transfer Learning, Domain Adaptation, Test-time Training, and Test-time Adaptation

Deep neural networks often experience performance degradation when deployed in environments different from their training settings, due to distribution shifts between source (training) and target (testing) domains. This issue has been extensively studied under the umbrella of transfer learning [15]–[17], which aims to transfer knowledge across domains. A key branch of transfer learning is domain adaptation (DA), where models trained on the labeled source domain are adapted to the target domain. Depending on the data availability, previous DA can be roughly classified into: Supervised DA [18] using labeled data in both source and target domains during training; Unsupervised DA [19]–[22], which relies on labeled source data and unlabeled target data simultaneously; and Source-free DA [23]–[25], that adapts to the target domain without access to source data, typically due to privacy constraints.

While traditional DA methods assume access to the entire target distribution before adaptation, real-world deployment often involves receiving data as an *online stream*, where samples arrive sequentially and the full distribution is never observed. This streaming nature of the target domain breaks the assumption of global access, making conventional domain adaptation infeasible. To handle this constraint, two prominent test-time adaptation paradigms have emerged. Online Test-time Training (OTTT) [26], [27] introduces an auxiliary task – often self-supervised – during pre-training. At test time, the model optimizes this auxiliary objective to adapt to the target distribution accordingly; Online Test-time Adaptation (OTTA) [3]–[8] poses a more demanding and practical scenario, where the model must adapt on-the-fly to the test stream without any prior modification during training. This setting emphasizes the need for rapid, real-time model updates to effectively capture the continuously incoming data.

TABLE I: Comparison of different transfer learning settings where \checkmark denotes settings closer to real-world conditions.

Research Fields	No Source Data*	No Target Labels*	Online Adaptation	Model Agnostic
Supervised Domain Adaptation	×	×	×	–
Unsupervised Domain Adaptation	×	✓	×	–
Source-free Domain Adaptation	✓	✓	×	–
Online Test-time Training	✓	✓	✓	×
Online Test-time Adaptation	✓	✓	✓	✓

A brief comparison of these adaptation settings is summarized in TABLE I. Our work falls under the OTTA setting, where we propose a generalizable and robust adaptation framework that maintains strong performance across diverse distribution shifts and corruptions – without relying on source data or altering the pre-training process.

B. Non-i.i.d. Test-time Adaptation

While conventional TTA methods primarily focus on single domain shifts under the idealized independent and identically distributed (i.i.d.) assumption, real-world deployment often violates these conditions due to inherent data heterogeneity. This discrepancy has motivated recent efforts to extend TTA to more realistic settings, with two primary challenges:

1) *Mixed Domains*: Modern TTA methods designed for continual domain shifts [5], [6], [9], [10], [28] have pushed beyond single adaptation problems. However, while they account for the dynamic target distribution shifts over time, they typically assume that each batch contains only a single domain shift. This simplifies the real-world scenario, where multiple distribution shifts may occur simultaneously, creating a mixed-domain environment that remains largely unexplored.

Existing approaches primarily focus on stabilizing model updates through periodic parameter resets [7], [9] or importance weighting of target samples [6], [9], [10], but these techniques are ill-equipped to disentangle and manage the complex interleaving of domain shifts, leading to degraded performance. In contrast, our work explicitly addresses mixed domains via frequency-space decomposition, which facilitates domain separation and proactive distribution alignment prior to model adaptation. While recent efforts like [7] acknowledge mixed distribution challenges under the broader “Dynamic Wild World” paradigm, their unified treatment of diverse real-world factors does not systematically address data heterogeneity. Conversely, our study directly targets the core issue of mixed domains in TTA, introducing tailored strategies for disentangling and adapting to co-occurring heterogeneous distributions.

2) *Dependent Sampling*: The second challenge arises from temporal-dependent sampling, which introduces class-level dependencies. This topic has garnered considerable research attention, with a growing body of work [28]–[33] actively addressing it through strategies such as pseudo-label-based rebalancing or extended observation windows. These approaches primarily aim to address temporal imbalances caused by skewed class distributions over time, aiming to improve target domain estimation by addressing low class diversity within

a batch. However, as these methods focus on within-domain temporal coherence, their applicability becomes limited when batches contain samples from multiple target domains. This limitation is also reflected in our experiments, where mixed-domain sampling poses notable challenges not accounted for in these approaches.

III. PROBLEM DEFINITION OF MIXED DOMAIN SHIFTS

Test-time adaptation (TTA) aims to adjust a model $q_\theta(y|x)$, initially trained on a source dataset $\mathcal{D}_s = \{(x, y) \sim p_s(x, y)\}$, to a target domain $\mathcal{D}_t = \{(x, y) \sim p_t(x, y)\}$ on a data stream without accessing source data or target labels. TTA handles covariate shift by assuming $p_s(y|x) = p_t(y|x)$ while $p_s(x) \neq p_t(x)$. This challenge intensifies when \mathcal{D}_t contains multiple non-i.i.d sub-distributions $p_{t_i}(x)$, such as

$$p_t(x) \leftarrow \{p_{t_1}(x), p_{t_2}(x), \dots, p_{t_N}(x)\}.$$

Specifically, we have $\mathcal{D}_t = \mathcal{D}_{t_1} \cup \mathcal{D}_{t_2} \cup \dots \cup \mathcal{D}_{t_N}$ where $x \in \mathcal{D}_{t_1}$ satisfying $x \sim p_{t_1}(x)$. This scenario requires the model $q_\theta(y|x)$ to effectively handle the heterogeneous and evolving target distribution to maintain robust performance. TTA strategies must therefore refine the model to optimize its predictive accuracy across these diverse sub-domains, ensuring consistent and reliable performance amidst significant distributional variability.

IV. UN-MIXING TTA UNDER MIXED DISTRIBUTION SHIFTS: A FOURIER PERSPECTIVE

While Test-Time Adaptation (TTA) methods perform well under single-type shifts, they degrade under mixed distribution shifts that are ubiquitous in real-world deployment (see Fig. 1 (b)). To address this, we advocate a paradigm of *proactive distribution management*: before any parameter update, we resolve heterogeneity by decomposing the input stream in frequency space. Our key insight is that different distributions leave distinct spectral footprints, which can be utilized to disentangle the heterogeneous data stream. As shown in Fig. 3, high-frequency components naturally separate different domain shifts, in contrast to the substantial overlap observed in the latent sample features from a pre-trained model. This proactive step transforms an ill-posed, entangled adaptation problem into a set of well-conditioned homogeneous subproblems.

Take TBN [34] as an example. In its original centralized version, TBN computes statistical information using the whole target batch and directly replaces the source values for online

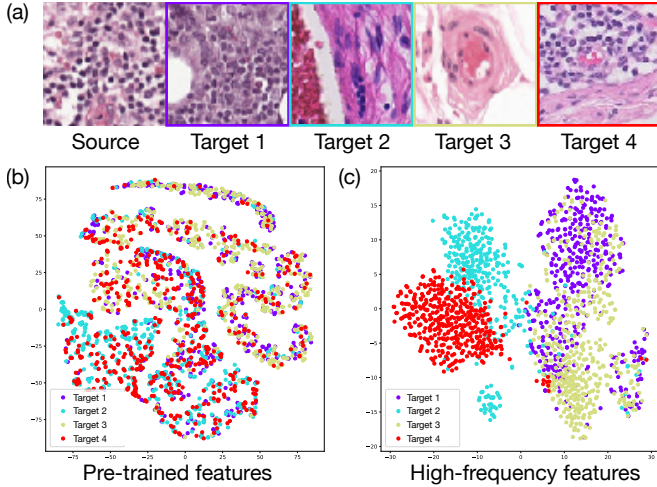


Fig. 3: (a) Example histopathology patches from five distinct healthcare centers illustrate visual heterogeneity across different domains (Camelyon17 [35]). (b) Latent features from the pre-trained model fail to distinguish target subdomains and remain highly entangled. (c) In contrast, high-frequency features can clearly separate different target subdomains.

adaptation. While effective under single-domain shifts, this whole-batch, homogeneous strategy produces biased statistics under mixed domain shifts, leading to suboptimal adaptation (see Fig. 4 (a)). In contrast, our decentralized approach first applies high-frequency clustering to partition the batch into locally homogeneous clusters. Batch normalization statistics are then computed within each cluster, enabling localized adaptation that can effectively prevent cross-domain contamination. Therefore, this decentralized strategy can reduce the error rate by a notable 4.27% and yields tighter within-class cohesion along with sharper between-class boundaries compared to centralized adaptation (see Fig. 4 (b)).

V. FREQUENCY-BASED DECENTRALIZED ADAPTATION

As outlined in the previous section, distinguishing samples from different distribution shifts provides a promising direction for TTA. Building on this insight, we introduce Frequency-based Decentralized Adaptation (FreDA), which partitions target samples in the Fourier space into homogeneous subdomains, enabling more accurate adaptation. We further enhance this process with a augmentation strategy that diversifies each subdomain in the Fourier space to improve model robustness.

A. Frequency-based Decentralized Learning

We first introduce Frequency-based Decentralized Learning framework. It begins by extracting high-frequency information from the pixel space to partition target samples into homogeneous subsets, disclosing the latent target subdomains contained within a batch. We then perform a decentralized adaptation, where multiple local models – sharing the same architecture – independently adapt to their assigned subsets. At regular intervals, the parameters of these local models

Methods	CIFAR-10-C	CIFAR-100-C	ImageNet-C
TBN (centralized)	33.8	45.8	82.5
TBN (our decentralized)	28.5	43.2	77.6

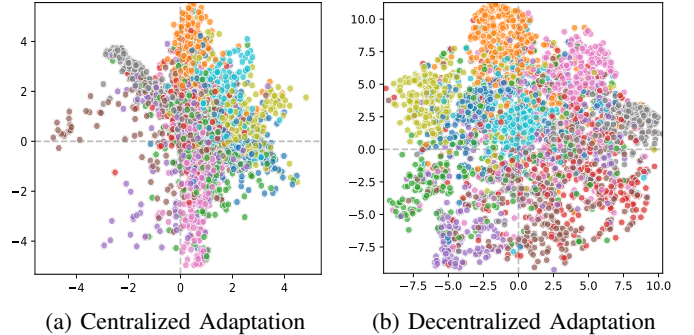


Fig. 4: Classification error rate (%) and t-SNE sample feature visualization using TBN [34] under mixed distribution shifts. Different colors denote different classes. (a) Original Centralized Adaptation: global Batch Normalization parameters are computed from the whole target batch. (b) Our Decentralized Adaptation: local Batch Normalization parameters are tailored for clusters separated based on high-frequency features. Decentralized adaptation achieves a 4.27% error reduction and clearer class structure compared with centralized adaptation.

are aggregated to form a stronger base model, which is subsequently used to update the local models for the next adaptation phase. Detailed procedures are provided in the following subsections.

1) *Frequency Feature Extraction*: We start by extracting frequency domain features from the input images. Let $\mathbf{X} \in \mathbb{R}^{n \times c \times h \times w}$ denote a batch of input images, where n is the batch size, c is the number of channels, h and w are the height and width. We first apply a Fourier transform \mathcal{F} to each image \mathbf{x}_i . This transform converts the image from the spatial domain to the frequency domain, producing a complex-valued representation $\mathcal{F}(\mathbf{x}_i) \in \mathbb{C}^{h \times w \times c}$ that contains both real $R(\mathbf{x}_i)$ and imaginary part $I(\mathbf{x}_i)$. Next, we compute the amplitude spectrum $A(\mathbf{x}_i)(u, v)$ using $A(x)(u, v) = \sqrt{R^2(x)(u, v) + I^2(x)(u, v)}$. It reveals the intensity of the frequency content, e.g., high-frequency amplitudes highlight edges and fine details while low-frequency amplitudes emphasize the overall structure and gradual changes. Then, we filter out low-frequency elements using mask $M(u, v) = \mathbb{1} \left(\left(u < \frac{h}{4} \vee u > \frac{3h}{4} \right) \vee \left(v < \frac{w}{4} \vee v > \frac{3w}{4} \right) \right)$ to emphasize the high-frequency components $G(x)(u, v)$ that are more likely to indicate shifts in distribution:

$$G(x)(u, v) = A(x)(u, v) \cdot M(u, v). \quad (1)$$

2) *Frequency-Based Clustering*: We then employ a clustering algorithm (e.g., K-means) to partition the frequency features into K clusters, each corresponding to a different type of distribution shift. The process is formalized as:

$$\min_{\mathbf{C}, \mathbf{Z}} \sum_{i=1}^n \|\mathbf{A}_{hf,i} - \mathbf{C}_{z_i}\|_2^2, \quad (2)$$

bank strategy [4], [28], [36], [37] that is updated in real time. This design serves two purposes: **1)** to ensure accurate clustering – since an overly small batch could impede the effective separation of data – and **2)** to maintain the number of samples processed by the local model consistent with the original batch size, thereby preventing performance degradation due to a drastic reduction in batch size (e.g., reducing by a factor of the cluster number).

VI. THEORETICAL INSIGHTS

To facilitate theoretical understanding of our method, we adopt the expansion-based framework [38], which offers a principled analysis of pseudo-labeling under local perturbations and neighborhood consistency, and connects these properties directly to upper bounds on model error rates. We first revisit the key definitions and theorems, then demonstrate how our method effectively tightens this generalization bound under mixed domain shifts from the viewpoints of *Frequency-coherent Partition* and *Augmentation-induced Expansion*.

A. Expansion Theory

Definition 1 ((a, c) -expansion). A class-conditional distribution P_i satisfies (a, c) -expansion if $\forall S \subseteq \mathcal{X}$ with $P_i(S) \leq a$:

$$P_i(\mathcal{N}(S)) \geq \min(cP_i(S), 1)$$

where $\mathcal{N}(S)$ refers to the neighborhood of S under data augmentations.

Definition 2 (Separation). P is (μ, r) -separated if:

$$\mathbb{E}_{x \sim \mathcal{P}} \left[\max_{x' \in B_r(x)} \mathbf{1}(G(x) \neq G(x')) \right] \leq \mu$$

where $B_r(x)$ is an ℓ_2 -ball of radius r .

The core theorem from [38] states:

Theorem 1 (Pseudo-label Denoising). Under (a, c) -expansion and (μ, r) -separation, any classifier G of:

$$\min_G \frac{c+1}{c-1} \mathcal{L}_{pl}(G) + \frac{2c}{c-1} \mathcal{R}_B(G)$$

achieves error:

$$\text{Err}(G) \leq \frac{2}{c-1} \text{Err}(G_{pl}) + \frac{2c}{c-1} \mu$$

\mathcal{L}_{pl} is pseudo-label loss and \mathcal{R}_B is consistency regularizer.

B. Analysis of Our Method

Our method reduces both terms in Theorem 1 to achieve a tighter bound from two perspectives:

1) *Frequency-based Partition*: Let $\{P_{t_k}\}_{k=1}^K$ be the K sub-domains derived from frequency-based partitioning. For the related measurable sets $\{S_k\}_{k=1}^K$ ($S_k \subseteq X_k$), we have:

$$\text{Err}(G_{pl}^k) \leq \text{Err}(G_{pl}) - \Delta_k$$

where $\Delta_k = \mathcal{P}_{t_k}(E_c)$ and $E_c = \{x \in X_k \mid G_{pl}(x) \neq y(x)\}$. This contributes to the reduction of the first term in Theorem 1, which is further supported by experimental results in Fig. 4.

2) *Augmentation-Induced Expansion*: Our frequency augmentation expands neighborhoods:

$$\widehat{\mathcal{N}}(S) = \mathcal{N}_{\text{base}}(S) \cup \left\{ x' : \inf_{x \in S} |A(\mathcal{F}(x')) - A(\mathcal{F}(x))|_2 \leq \epsilon \right\}$$

where $\mathcal{N}_{\text{base}}(S)$ is the base augmentation neighborhood. It is worth noting that, unlike most methods, we do not apply base augmentation. The term $\mathcal{N}_{\text{base}}(S)$ is retained in the formulation for theoretical completeness. Our choice of this representation is intended to highlight the expansion gain brought by incorporating frequency augmentation. The expansion gain becomes:

$$\widehat{c} = c_{\text{base}} + \gamma, \quad \gamma = \inf_{S: P(S) \leq a} \frac{P(\widehat{\mathcal{N}}(S) \setminus \mathcal{N}_{\text{base}}(S))}{P(S)}$$

Substituting into Theorem 1, the error becomes:

$$\begin{aligned} \text{Err}(G) &\leq \underbrace{\frac{2}{(c_{\text{base}} + \gamma) - 1} \left(\text{Err}(G_{pl}) - \sum_{k=1}^K \Delta_k \right)}_{\text{Reduced by both terms}} \\ &\quad + \underbrace{\frac{2(c_{\text{base}} + \gamma)}{(c_{\text{base}} + \gamma) - 1} \mu}_{\text{Reduced by } O(\gamma/c^2)} \end{aligned}$$

Remark. By leveraging frequency-based decentralized learning and augmentation, our method addresses the key components in the expansion-theoretic error, yielding a provably tighter generalization bound that supports more challenging online adaptation scenarios under diverse distribution shifts.

Notation

- c : Expansion factor (Def. 1).
Class-wise connectivity metric: Larger c implies stronger neighborhood propagation of local consistency to global predictions.
- μ : Inter-class separation probability (Def. 2).
Robustness measure: Probability of different classes having overlapping neighborhoods under perturbations, lower μ indicates clearer decision boundaries.
- \mathcal{R}_B : Consistency regularizer (Thm. 1).
Stability term: Penalizes prediction inconsistency between original inputs and their augmented variants.
- Δ_k : Error reduction in k -th sub-domain.
Specialization gain: Reduced pseudo-label noise in sub-domain k due to frequency-based partitioning.
- γ : Expansion gain from frequency augmentation.
Neighborhood enhancement: Additional expansion capability measured as the relative increase of augmented neighborhoods.

VII. EXPERIMENTS

A. Datasets and Experimental Setup

1) *Datasets*: To provide a comprehensive evaluation of TTA deployment, we test models under three different scenarios (see Fig. 3 and Appendix VIII-C for visualizations):

- **Common Image Corruptions**: We evaluate models on CIFAR-10-C, CIFAR-100-C, and ImageNet-C [39] with 10, 100 and 1000 classes, respectively. These benchmarks

TABLE II: Classification error rate (\downarrow) on CIFAR-10-C, CIFAR-100-C, ImageNet-C under **Mixed Distribution Shifts**.

Methods	Gauss.	Shot	Impul.	Defoc.	Glass	Motion	Zoom	Snow	Frost	Fog	Brig.	Contr.	Elast.	Pixel	JPEG	Avg.
CIFAR-10-C	72.3	65.7	72.9	46.9	54.3	34.8	42.0	25.1	41.3	26.0	<u>9.3</u>	46.7	26.6	58.4	30.3	43.5
TBN	45.5	42.8	59.7	34.2	44.3	29.8	32.0	19.8	21.1	21.5	<u>9.2</u>	27.9	33.1	55.5	30.8	33.8
TENT	73.5	70.1	81.4	31.6	60.3	29.6	28.5	30.8	35.3	25.7	<u>13.6</u>	44.2	32.6	70.2	34.9	44.1
ETA	36.2	33.3	52.3	22.9	38.9	22.4	20.5	19.5	19.7	20.4	11.3	35.4	26.6	38.8	<u>25.1</u>	28.2
AdaContrast	36.7	34.3	48.8	18.2	39.1	21.1	<u>17.7</u>	<u>18.6</u>	<u>18.3</u>	<u>16.8</u>	9.0	<u>17.4</u>	27.7	44.8	24.9	<u>26.2</u>
CoTTA	38.7	36.0	56.1	36.0	36.8	32.3	31.0	19.9	17.6	27.2	11.7	52.6	30.5	35.8	25.7	32.5
SAR	45.5	42.7	59.6	34.1	44.3	29.7	31.9	19.8	21.1	21.5	<u>9.3</u>	27.8	33.0	55.4	30.8	33.8
RoTTA	60.0	55.5	70.0	23.8	44.1	<u>20.7</u>	21.3	20.2	22.7	16.0	<u>9.4</u>	22.7	27.0	58.6	29.2	33.4
RDumb	<u>34.9</u>	<u>32.3</u>	49.4	23.3	<u>38.2</u>	<u>23.3</u>	20.7	19.9	19.3	20.7	11.2	29.3	<u>26.7</u>	41.5	25.2	27.7
DeYO	45.8	42.3	65.7	21.3	41.8	25.1	19.5	21.1	19.6	19.2	12.3	21.8	28.5	39.3	28.0	30.1
UnMix-TNS	50.0	44.4	44.3	34.4	48.2	32.7	30.0	35.5	35.9	47.5	28.1	38.7	43.9	40.0	43.3	39.8
FreDA (ours)	23.1	22.2	32.2	<u>18.7</u>	41.6	18.8	16.8	17.9	19.9	16.9	9.8	13.2	29.1	35.4	28.6	22.9
CIFAR-100-C	73.0	68.0	39.4	29.3	54.1	30.8	<u>28.8</u>	39.5	45.8	50.3	29.5	55.1	37.2	74.7	41.2	46.4
TBN	62.7	60.7	43.1	35.5	50.3	35.7	34.4	39.9	51.5	27.5	45.5	42.3	72.8	46.4	45.8	45.8
TENT	95.6	95.2	89.2	72.8	82.9	74.4	72.3	78.0	79.7	84.7	71.0	88.5	77.8	96.8	78.7	82.5
ETA	42.6	40.3	34.1	30.3	42.4	32.0	29.4	<u>35.6</u>	<u>35.8</u>	44.1	30.2	41.8	36.9	38.9	40.9	37.0
AdaContrast	54.5	51.5	37.6	30.7	45.4	32.1	30.3	<u>36.9</u>	<u>36.5</u>	45.3	<u>28.0</u>	42.7	38.2	75.4	41.7	41.8
CoTTA	54.4	52.7	49.8	36.0	45.8	36.7	33.9	38.9	<u>35.8</u>	52.0	<u>30.4</u>	60.9	40.2	<u>38.0</u>	41.1	43.1
SAR	75.8	72.7	41.1	29.2	45.2	<u>31.1</u>	28.9	36.7	<u>37.7</u>	43.9	29.3	41.8	<u>37.1</u>	89.2	42.4	45.5
RoTTA	65.0	62.3	39.3	33.4	50.0	<u>34.2</u>	32.6	36.6	<u>36.5</u>	45.0	26.4	<u>41.6</u>	<u>40.6</u>	89.5	48.5	45.4
RDumb	<u>42.3</u>	<u>40.0</u>	34.1	30.5	<u>42.4</u>	31.9	29.5	35.7	35.9	43.6	30.4	<u>41.9</u>	36.9	38.1	<u>40.5</u>	<u>36.9</u>
DeYO	57.2	53.4	38.8	34.7	47.3	37.3	34.1	40.8	40.5	50.6	33.3	45.8	41.5	94.5	45.7	46.4
UnMix-TNS	65.8	64.1	46.4	37.5	51.7	36.0	36.4	38.5	39.4	51.1	29.3	42.8	43.2	67.8	49.4	46.6
FreDA (ours)	34.8	34.7	<u>36.6</u>	<u>29.4</u>	41.2	29.9	28.4	33.8	33.7	<u>41.1</u>	29.8	34.9	36.9	37.1	38.7	34.7
ImageNet-C	97.8	97.1	98.2	81.7	89.8	85.2	77.9	83.5	77.1	75.9	<u>41.3</u>	94.5	82.5	79.3	68.6	82.0
TBN	92.8	91.1	92.5	87.8	90.2	87.2	82.2	82.2	82.0	79.8	48.0	92.5	83.5	75.6	70.4	82.5
TENT	99.2	98.7	99.0	90.5	95.1	90.5	84.6	86.6	84.0	86.5	46.7	98.1	86.1	77.7	72.9	86.4
ETA	90.7	89.2	90.5	<u>77.0</u>	80.6	74.0	68.9	72.4	<u>70.3</u>	64.6	43.9	93.4	69.2	52.3	55.9	<u>72.9</u>
AdaContrast	96.2	95.5	96.2	93.2	96.4	96.3	90.5	92.7	91.9	92.4	50.8	97.0	96.6	89.7	87.1	90.8
CoTTA	89.1	86.6	<u>88.5</u>	80.9	87.2	81.1	75.8	73.3	75.2	70.5	41.6	85.0	78.1	65.6	61.6	76.0
SAR	98.4	97.3	98.0	84.0	87.3	82.6	77.2	77.5	76.1	72.5	43.1	96.0	78.3	61.8	60.4	79.4
RoTTA	89.4	88.6	89.3	83.4	89.1	86.2	80.0	78.9	76.9	74.2	37.4	89.6	79.5	69.0	59.6	78.1
RDumb	<u>89.0</u>	87.6	88.6	78.1	82.3	75.2	70.1	73.0	71.0	65.1	43.9	92.6	<u>70.7</u>	<u>53.7</u>	<u>56.3</u>	73.1
DeYO	99.5	99.2	99.5	89.5	95.0	83.9	78.8	75.0	87.8	79.2	47.3	99.2	92.4	59.0	60.4	83.0
UnMix-TNS	91.7	92.8	91.7	92.3	93.4	91.5	84.8	86.3	84.1	85.0	62.0	96.5	88.6	81.7	77.3	86.7
FreDA (ours)	72.4	74.0	71.4	76.5	<u>82.3</u>	72.1	64.1	64.4	64.8	59.1	43.7	79.7	71.0	54.2	58.6	67.2

Note: WRN-28, ResNeXt-29, and ResNet-50 backbones are used for CIFAR-10-C, CIFAR-100-C, and ImageNet-C, respectively.

are designed to assess the model robustness against various corruptions. Each dataset consists of 15 distinct corruptions across five severity levels, resulting in 150,000 at each severity for CIFAR-10-C/100-C, and 750,000 for ImageNet-C.

- Natural Domain Shifts: We extend evaluation to DomainNet126 [40], which presents natural shifts across four domains (Real, Clipart, Painting, Sketch) encompassing 126 classes as a subset of the larger DomainNet dataset.
- Medical Application: Models are further evaluated on Camelyon17 [35], comprising over 450,000 histopathological patches from lymph node sections for binary classification of normal and tumor tissue, with data originating from five distinct healthcare centers.

For corruption datasets, the model is pretrained on the clean dataset and the 15 corruptions are randomly mixed as the target distribution. We leverage the highest severity = 5 in all the experiments. In DomainNet126 and Camelyon17, one subdomain is selected as the source, and the others serve as mixed target distributions. All reported results are averaged over runs with fixed seeds (0, 1, and 2).

2) *Baselines*: We compare FreDA with 10 models, including TBN [34], TENT [3], CoTTA [5], ETA [6], SAR [7], AdaContrast [4], RoTTA [28], RDumb [9], DeYO [10], and UnMix-TNS [31]. TBN [34] re-estimates batch normalization statistics from test data. TENT [3] minimizes prediction entropy to optimize batch normalization. CoTTA [5] addresses long-term test-time adaptation in changing environ-

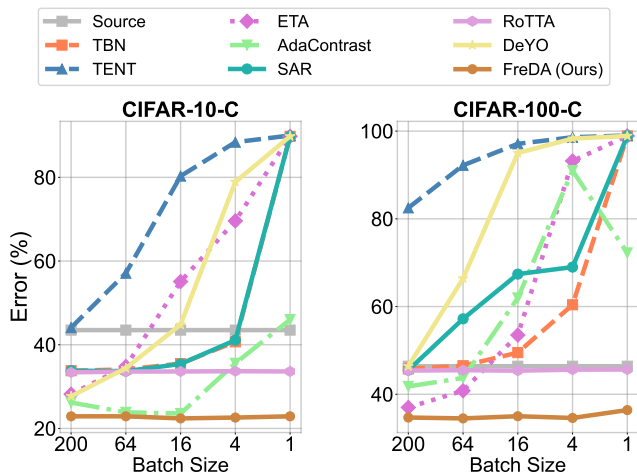
ments. ETA [6] and SAR [7] exclude unreliable and redundant samples during optimization. AdaContrast [4] utilizes contrastive learning to refine pseudo-labels and improve feature learning. RoTTA [28] presents a robust batch normalization scheme with a memory bank for category-balanced estimation. RDumb [9] leverages weighted entropy and periodically resets the model to its pretrained state to prevent collapse. DeYO [10] quantifies the impact of object-destructive transformations for sample selection and weighting. UnMix-TNS [31] introduces a test-time normalization layer for non-i.i.d. environments by decomposing BN statistics. For fair comparisons, we conduct experiments using the open source online TTA repository [41]¹, which provides codes and configurations of state-of-the-art TTA methods.

3) *Hyperparameter Configuration*: The adaptation batch size is set to 200, 64, 128 and 32 for CIFAR-10/100-C, ImageNet-C, DomainNet126 and Camelyon17 following the previous methods. The SGD optimizer is used with learning rates adjusted to 0.01, 0.0001, 0.001 and 0.00005, respectively. The learning rate is proportionally decreased in the experiment studying the effect of batch size. The Kmeans Size is 512, Clutser Number is 4, Communication Interval is 10 across all the tasks. The perturbation magnitude α is fixed to 0.1 and the coefficient λ in loss function is fixed to 0.5. Two threshold in Eq. 5 is set to the same value for corruption datasets and DomainNet126 following ETA [6]. While for Camelyon17, the

¹<https://github.com/mariodoebler/test-time-adaptation>

TABLE III: Classification error rate (\downarrow) on DomainNet126 and Camelyon17 under **Mixed Distribution Shifts**.

DomainNet126						Camelyon17					
Methods	Real	Painting	Clipart	Sketch	Avg.	C1	C2	C3	C4	C5	Avg.
Source	45.2	41.6	49.5	45.3	45.4	21.6	43.6	52.5	47.4	47.6	42.5
TBN	45.5	39.9	45.9	37.5	42.2	26.5	38.5	31.7	39.4	<u>32.8</u>	<u>33.8</u>
TENT	42.2	37.8	44.7	37.5	40.6	44.7	50.5	49.9	49.1	48.6	48.6
ETA	41.1	37.3	43.4	36.4	39.5	47.4	52.5	47.9	49.9	39.2	47.4
SAR	43.2	38.5	44.8	37.0	40.9	26.5	<u>38.5</u>	<u>31.7</u>	39.4	<u>32.8</u>	<u>33.8</u>
DeYO	40.9	36.4	43.6	36.9	39.4	50.4	50.3	48.8	51.7	50.5	50.4
FreDA (ours)	40.2	36.1	40.0	33.6	37.5	18.6	24.7	24.8	<u>40.5</u>	30.8	27.9

Fig. 5: Classification error rate (\downarrow) on CIFAR-10-C/100-C with various batch size under **Mixed Distribution Shifts**.

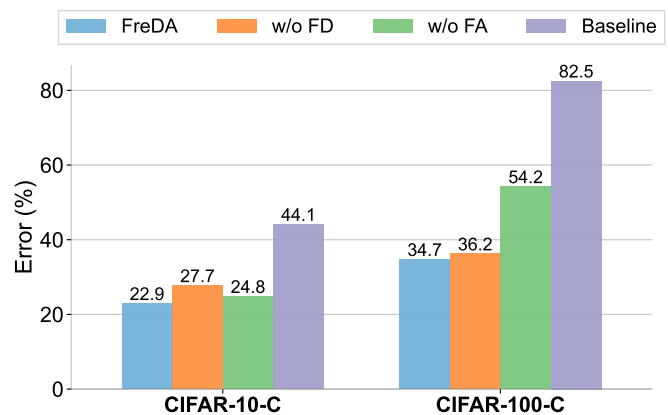
class diversity related threshold is adjusted to 0.9 empirically.

4) *Implementation Details*: We utilize models from RobustBench [42], including WildResNet-28 [43] for CIFAR-10-C and ResNeXt-29 [44] for CIFAR-100-C, both pretrained by [45]. For ImageNet-C, the pretrained ResNet-50 [46] is obtained from torchvision. For DomainNet126, pretrained ResNet-50 is sourced from AdaContrast [4], while for Camelyon17, we train a DenseNet-121 [47] from scratch to 100 epochs with other training specifications outlined in the Wilds benchmark [48]. Our implementation can be found at <https://github.com/kiwi12138/FreDA>.

B. Main Results

1) *FreDA improves across diverse distribution shifts*: Our method consistently attains the lowest error rates across all evaluated datasets (see TABLE II and III). Notably, on the Camelyon17 dataset, FreDA reduced the error rate to 27.9%, outperforming the next best method by 5.9%. This significant improvement is particularly notable where other approaches falter if compared with no training (TBN), meaning they struggle to adapt to the complex medical imaging data. By effectively handling high variability and intricate patterns in the data, FreDA maintains superior accuracy and adaptability.

2) *FreDA remains stable under various batch size*: To simulate deployment with constrained batch sizes, we evaluate models under both varying batch sizes and mixed distributions. In Fig. 5, we present the results on CIFAR-10-C and

Fig. 6: Classification error rate (\downarrow) on CIFAR-10-C/100-C with various batch size under **Mixed Distribution Shifts**.

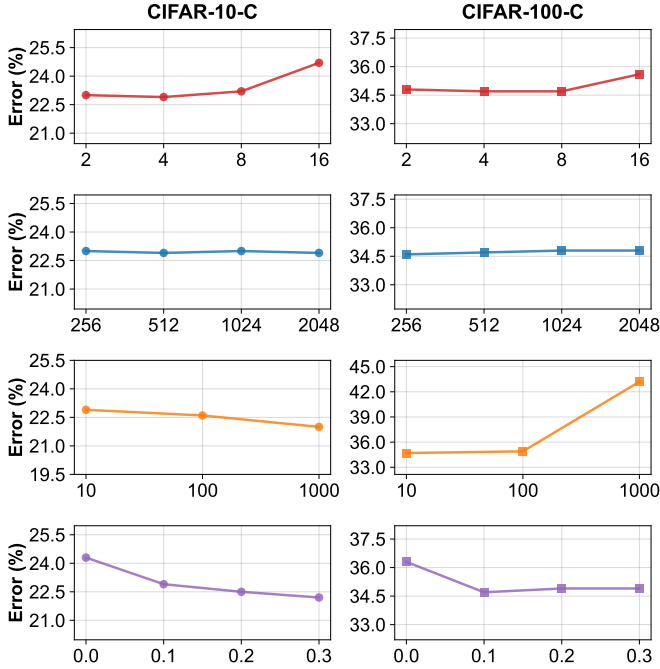
CIFAR-100-C using batch sizes ranging from 200 down to 1. Unlike other methods that significantly degrade as batch size decreases – for example the error rate of DeYO increases from 27.7% to 89.8% when batch size drops from 200 to 1 on CIFAR-10-C – FreDA consistently maintains strong performance. This stability demonstrates FreDA’s robustness, making it highly suitable for real-world applications where large batches is not always feasible.

3) *FreDA enhances adaptation via frequency-based designs*: This section validates our designs by ablating two key modules – Frequency-based Decentralized learning (FD) and Frequency-based Augmentation (FA) – from the full model. It is worth mentioning that our FreDA is built upon TENT (our baseline) by integrating both FD and FA. From Fig. 6, we observe the following: **a)** Removing FD leads to a clear performance drop, underscoring the importance of our proposed decentralized adaptation paradigm in handling mixed distribution shifts. **b)** Removing FA results in a surprisingly large error rate increase on CIFAR-100-C. In more challenging classification scenarios (e.g., CIFAR-100-C vs. CIFAR-10-C), the target domain typically exhibits sparser class-wise coverage. Augmentation enriches the target sample diversity while preserving semantic consistency, thereby mitigating overfitting to spurious patterns and enhancing robustness under severe and complex distribution shifts. Nevertheless, even without FA, our method still significantly outperforms the baseline model, further confirming the critical role of our decentralized adaptation framework.

4) *FreDA adapts robustly to hyperparameter variations*: We investigate the impact of the key hyperparameters:

TABLE IV: Classification error rate (\downarrow) on ImageNet-C under **Mixed Distribution Shifts** using ViT-Base backbone.

Methods	Gauss.	Shot	Impul.	Defoc.	Glass	Motion	Zoom	Snow	Frost	Fog	Brig.	Contr.	Elast.	Pixel	JPEG	Avg.
IN-C (ViTBase-LN)	65.8	67.3	65.3	68.8	74.4	64.3	66.6	56.8	45.2	48.6	29.2	81.8	57.1	60.8	50.2	60.2
TENT	60.6	60.4	59.6	63.6	67.8	57.1	61.2	55.0	48.8	47.4	28.6	66.7	53.9	50.4	44.4	55.0
ETA	59.3	57.8	57.9	58.8	62.8	52.5	58.2	51.0	46.4	44.2	28.8	58.3	51.1	46.9	41.9	51.7
AdaContrast	64.8	63.4	63.3	72.8	76.6	73.7	74.6	67.7	48.0	89.6	30.2	93.2	60.8	57.3	46.3	65.5
CoTTA	89.4	92.0	88.9	93.6	92.6	90.6	86.5	94.9	88.2	86.6	75.8	96.5	85.7	93.5	84.6	89.3
SAR	58.9	57.6	57.6	59.4	63.6	53.0	58.5	52.3	47.1	45.4	28.3	61.6	51.4	47.4	42.0	52.3
RoTTA	64.4	65.6	63.7	67.6	71.3	59.8	64.1	52.7	43.5	48.6	27.9	78.5	54.3	60.4	50.1	58.2
RDumb	59.7	58.5	58.5	60.0	64.1	54.0	59.0	52.0	46.7	44.5	28.6	61.2	51.9	48.3	42.6	52.6
DeYO	60.0	58.6	58.8	58.8	62.4	61.9	50.9	46.7	51.9	45.2	29.7	55.7	51.6	45.8	42.8	52.1
FreDA (ours)	55.9	53.7	55.0	58.0	57.9	50.9	57.4	45.5	42.9	43.9	29.5	51.7	47.8	41.6	40.7	48.8

Fig. 7: Parameter study with respect to CLUSTER_NUM, KMEANS_SIZE, COMM_INTERVAL & PERT_MAGNITUDE (from top to bottom) under **Mixed Distribution Shifts**.

CLUSTER_NUM, KMEANS_SIZE, COMM_INTERVAL, and PERT_MAGNITUDE. From Fig. 7, we have the following observations: **a)** CLUSTER_NUM is largely insensitive in the range of 2–8: performance varies only marginally across CIFAR10/100-C and remains stable on average, with a clear drop emerging only at the extreme setting of 16. We attribute the degradation at 16 to over-partitioning, where the model tends to overfit to subtle, cluster-specific variations rather than capturing domain-invariant patterns. Therefore, a moderate number of clusters, around 4, appears to strike a good balance between adaptation flexibility and maintaining model robustness. **b)** Varying KMEANS_SIZE from 256 to 2048 results in stable performance across all datasets, indicating that our method is robust to changes in cluster sizes. **c)** Our approach shows general robustness to communication frequency (varying COMM_INTERVAL from 10 to 1,000). On simpler datasets such as CIFAR10-C, infrequent communication (e.g., interval $f = 1000$) performs best, likely due to effective independent learning. In contrast, for complex datasets (e.g. CIFAR100-C), more frequent communication (e.g., $f = 10$)

TABLE V: Classification error rate (\downarrow) on CIFAR-10-C (C10), CIFAR-100-C (C100), and ImageNet-C (IN) using ResNet-50 & ViT-Base backbones under **Continual Setting**, averaged over 15 corruptions.

Methods	C10	C100	IN(ResNet)	IN(ViT)
Source	43.5	46.5	82.0	60.2
TBN	20.4	35.4	68.6	-
TENT	20.0	62.2	62.6	54.5
ETA	17.9	32.2	60.2	49.8
AdaContrast	18.5	33.5	65.5	57.0
CoTTA	16.5	32.8	63.1	77.0
SAR	20.4	32.0	61.9	51.7
RoTTA	19.3	34.8	67.3	58.3
RDumb	17.8	34.1	90.6	50.2
DeYO	87.0	98.1	90.6	94.3
UnMix-TNS	24.9	32.7	75.4	-
FreDA (ours)	19.5	32.5	60.2	47.9

improves performance, likely by mitigating divergence among local branches and ensuring model consistency. **d)** Introducing perturbation (PERT_MAGNITUDE) from 0 to a positive value yields a clear performance gain, confirming the effectiveness of our frequency-based augmentation strategy. Furthermore, when varying the magnitude between 0.1 and 0.3, FreDA maintains robust performance across datasets, indicating its resilience to moderate perturbation levels.

C. Performance with Transformer Backbone

In addition to evaluating our model on commonly compared CNN backbones, we further assess its performance under transformer-based architecture, specifically using the ViT-Base backbone. Here, we report results on the ImageNet-C benchmark using ViTBase-LN [49] (see TABLE IV), where the pretrained weights are obtained from torchvision. Importantly, all experimental configurations are kept consistent with those used in the CNN-based experiments. As shown, our method continues to deliver strong performance, demonstrating its robustness and adaptability across different backbone architectures.

D. Performance under Continual Settings

Although our method is specifically designed for mixed domain scenarios, we also evaluated its performance under the conventional continual test-time adaptation [3], [5] setting to assess its robustness in different contexts. In this setting, the model adapts online to a sequence of test domains without explicit knowledge of domain shifts, with only one

distribution shift occurring at a time and not reappearing. Without adjusting any parameters, our method demonstrated competitive performance compared to current state-of-the-art approaches. Notably, while UnMix-TNS effectively addresses non-i.i.d. issues (dependent sampling at the class level), it is less effective under i.i.d. conditions. Our results suggest that the proposed FreDA not only excels in its intended mixed domain scenarios but also generalizes effectively to standard continual adaptation tasks, providing a robust solution across various distributional challenges.

VIII. MORE DETAILS AND DISCUSSION

A. Adaptation Scenarios

1) *Mixed Domains*: In this scenario, the model processes a long sequence of test samples where each sample $x_i \sim p_{e_i}(x)$ is independently drawn from a randomly selected target domain $\mathcal{D}_{e_i} \in \{\mathcal{D}_{t_1}, \mathcal{D}_{t_2}, \dots, \mathcal{D}_{t_N}\}$ and a randomly selected class c_i among classes $\{1, 2, \dots, C\}$. The sequence is represented as:

$$\left\{ x_1^{\mathcal{D}_{e_1}, c_1}, x_2^{\mathcal{D}_{e_2}, c_2}, \dots, x_k^{\mathcal{D}_{e_k}, c_k} \right\},$$

where each target domain index $e_i \in \{1, 2, \dots, N\}$ and class number $c_i \in \{1, 2, \dots, C\}$ are independently and randomly selected for each sample x_i .

2) *Continual Domain Adaptation*: In this setting, the model adapts online to a sequentially presented series of test domains, where each domain shift occurs only once and does not reappear. The sequence progresses through distinct target domains in a fixed order $D_1 \rightarrow D_2 \rightarrow \dots \rightarrow D_N$, with samples from each domain appearing contiguously. The class labels within each domain are independently and randomly selected. The sequence is structured as:

$$\begin{aligned} & \underbrace{\{(x_1^{D_1, c_1}), (x_2^{D_1, c_2}), \dots, (x_{l_1}^{D_1, c_{l_1}})\}}_{\text{Samples from domain } D_1} \\ & \rightarrow \underbrace{\{(x_{l_1+1}^{D_2, c_{l_1+1}}), \dots, (x_{l_1+l_2}^{D_2, c_{l_1+l_2}})\}}_{\text{Samples from domain } D_2} \\ & \rightarrow \dots \rightarrow \underbrace{\{(x_{l_1+\dots+l_{N-1}+1}^{D_N, c_{l_1+\dots+l_{N-1}+1}}), \dots, (x_k^{D_N, c_k})\}}_{\text{Samples from domain } D_N} \end{aligned}$$

where:

- D_i denotes the i -th target domain in the fixed sequence, with $i \in \{1, 2, \dots, N\}$.
- $c_m \in \{1, 2, \dots, C\}$ is the randomly selected class label for the m -th sample, independent of domain transitions.

B. Further Remarks on Related Works

1) *Relation to Frequency Domain Learning*: Recent advances highlight frequency-based techniques as powerful tools for domain transfer. In domain generalization, frequency analysis has revealed critical insights into model robustness and learning dynamics [50]–[57]. For domain adaptation, interpolating image amplitude spectra across styles has proven effective in reducing domain gaps and preventing overfitting to low-level statistics [58]–[61]. Motivated by these advancements,

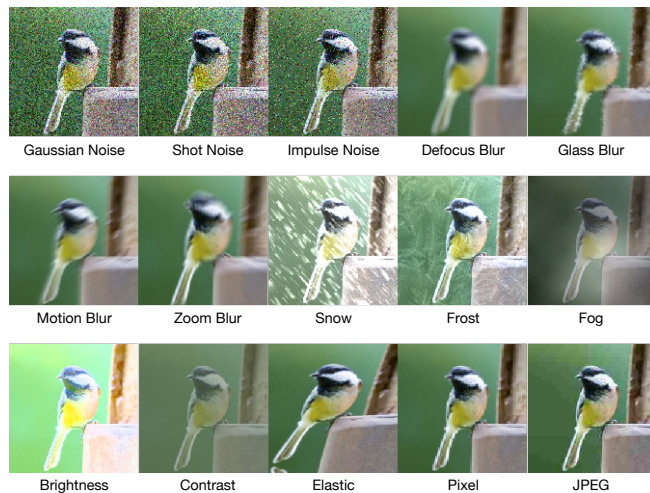


Fig. 8: Examples from ImageNet-C under image corruptions. The images showcase a range of corruption types (e.g., noise, blur, and weather distortions) at varying severity levels.

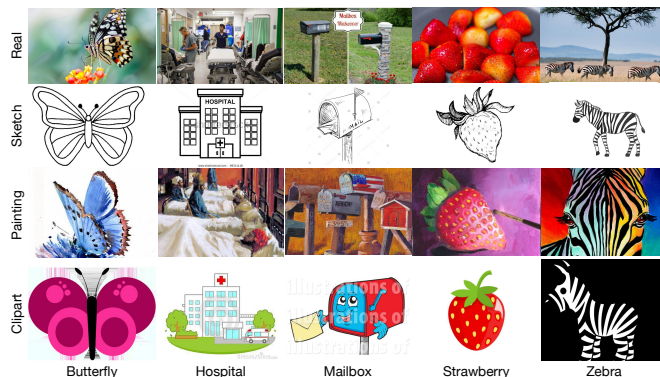


Fig. 9: Samples from DomainNet126 across four subdomains (Real, Sketch, Painting, Clipart). These visualizations reflect the stylistic and perceptual variations inherent in each domain.

we discover that frequency information inherently captures domain characteristics, making it a valuable medium for decoupling mixed target domains – an aspect largely unexplored in prior work. On this basis, we propose FreDA, addressing TTA under mixed domain shifts in Fourier space, with a decentralized adaptation and perturbation mechanism.

2) *Relation to Multi-Target Domain Adaptation*: TTA under mixed distribution shifts shares similarities with multi-target unsupervised domain adaptation (MT-UDA) [11]–[13], [62]–[64], yet diverges critically in complexity: while MT-UDA assumes static, predefined target domains and leverages labeled source data for explicit domain alignment, TTA operates with no access to source data and must adapt to dynamic, unpredictable target streams in an online manner. This eliminates direct source-target discrepancy computation and demand robust incremental adaptation rather than offline multi-domain optimization. These differences highlight the need for novel methodologies tailored specifically to TTA, going beyond the solutions developed for MT-UDA.

3) *Relation to Decentralized, Federated, Distributed Learning*: This work also intersects with decentralized, federated, and distributed learning due to splitting data batches into disjoint subsets and applying decentralized model adaptation. First, while decentralized learning focuses on non-i.i.d. data that is naturally distributed across multiple nodes [65], our approach starts with a centralized batch of target samples. By proactively splitting this data into disjoint subsets, we expose latent non-i.i.d. characteristics, enabling the effective use of decentralized learning techniques. Second, federated learning considers data privacy and model collaborations within decentralized learning [66]. In our case, as target samples are mixed in a batch, data privacy is not a concern. However, similar to federated learning, our approach also involves weight aggregation over subnetworks to enhance their base models. Third, distributed learning aims to improve training efficiency on large-scale datasets by partitioning data for synchronized training [67]. In contrast, our method operates in a real-time fine-tuning context with limited data at one time, hence scalability is less of a concern.

C. Dataset Visualization

To further illustrate the characteristics of the datasets used in our evaluation, we present visualizations of the data distribution across different corruption types (Fig. 8), natural domain shifts (Fig. 9), and medical centers (Fig. 3). These figures highlight the diverse challenges that our models face in each evaluation scenario, providing insight into the complexity of the test conditions.

IX. CONCLUSION

This paper advances Test-Time Adaptation by tackling the practical challenges posed by heterogeneous data streams. We introduce FreDA, a frequency-based decentralized adaptation framework that partitions incoming samples and performs localized adaptation, while employing distribution-aware augmentation to effectively handle mixed distribution shifts. Empirical results across multiple benchmarks demonstrate the effectiveness of our approach, highlighting its potential to drive future research on adapting to dynamic and diverse domain shifts.

Future Work: FreDA provides a principled framework for adapting to mixed distribution shifts, and we believe several promising directions could further enhance its capabilities. First, beyond the current proactive clustering, future work could investigate adaptive, learnable partitioning strategies that dynamically refine subset boundaries and better capture subtle relationships among target subdomains. Second, our frequency-based augmentation is currently applied at the sample level, which is well-suited for classification. Extending it to patch-level operations in spatial–frequency space may enrich the model’s granularity and open new possibilities for fine-grained tasks such as segmentation. Together, these directions offer natural extensions to broaden FreDA’s applicability in increasingly realistic and dynamic environments.

REFERENCES

- [1] M. Long, J. Wang, G. Ding, J. Sun, and P. S. Yu, “Transfer feature learning with joint distribution adaptation,” in *Proceedings of the IEEE International Conference on Computer Vision*, 2013, pp. 2200–2207.
- [2] Y. Ganin and V. Lempitsky, “Unsupervised domain adaptation by backpropagation,” in *International Conference on Machine Learning*. PMLR, 2015, pp. 1180–1189.
- [3] D. Wang, E. Shelhamer, S. Liu, B. Olshausen, and T. Darrell, “Tent: Fully test-time adaptation by entropy minimization,” in *International Conference on Learning Representations*, 2021.
- [4] D. Chen, D. Wang, T. Darrell, and S. Ebrahimi, “Contrastive test-time adaptation,” in *Proceedings of the IEEE/CVF Conference on Computer Vision and Pattern Recognition*, 2022, pp. 295–305.
- [5] Q. Wang, O. Fink, L. Van Gool, and D. Dai, “Continual test-time domain adaptation,” in *Proceedings of the IEEE/CVF Conference on Computer Vision and Pattern Recognition*, 2022, pp. 7201–7211.
- [6] S. Niu, J. Wu, Y. Zhang, Y. Chen, S. Zheng, P. Zhao, and M. Tan, “Efficient test-time model adaptation without forgetting,” in *International Conference on Machine Learning*. PMLR, 2022, pp. 16 888–16 905.
- [7] S. Niu, J. Wu, Y. Zhang, Z. Wen, Y. Chen, P. Zhao, and M. Tan, “Towards stable test-time adaptation in dynamic wild world,” in *International Conference on Learning Representations*, 2023.
- [8] Z. Su, J. Guo, K. Yao, X. Yang, Q. Wang, and K. Huang, “Unraveling batch normalization for realistic test-time adaptation,” in *Proceedings of the AAAI Conference on Artificial Intelligence*, vol. 38, no. 13, 2024, pp. 15 136–15 144.
- [9] O. Press, S. Schneider, M. Kümmerer, and M. Bethge, “Rdumb: A simple approach that questions our progress in continual test-time adaptation,” *Advances in Neural Information Processing Systems*, vol. 36, 2024.
- [10] J. Lee, D. Jung, S. Lee, J. Park, J. Shin, U. Hwang, and S. Yoon, “Entropy is not enough for test-time adaptation: From the perspective of disentangled factors,” in *International Conference on Learning Representations*, 2024.
- [11] T. Isobe, X. Jia, S. Chen, J. He, Y. Shi, J. Liu, H. Lu, and S. Wang, “Multi-target domain adaptation with collaborative consistency learning,” in *Proceedings of the IEEE/CVF conference on computer vision and pattern recognition*, 2021, pp. 8187–8196.
- [12] H. Yu, M. Hu, and S. Chen, “Multi-target unsupervised domain adaptation without exactly shared categories,” *arXiv preprint arXiv:1809.00852*, 2018.
- [13] Q. Tian, C. Ma, M. Cao, J. Wan, Z. Lei, and S. Chen, “Unsupervised multitarget domain adaptation with dictionary-bridged knowledge exploitation,” *IEEE Transactions on Neural Networks and Learning Systems*, vol. 35, no. 3, pp. 3464–3477, 2024.
- [14] K. Yao, Z. Tan, Z. Su, X. Yang, J. Sun, and K. Huang, “Scmix: Stochastic compound mixing for open compound domain adaptation in semantic segmentation,” *IEEE Transactions on Neural Networks and Learning Systems*, 2025.
- [15] S. J. Pan and Q. Yang, “A survey on transfer learning,” *IEEE Transactions on Knowledge and Data Engineering*, vol. 22, no. 10, pp. 1345–1359, 2009.
- [16] L. Zhang and X. Gao, “Transfer adaptation learning: A decade survey,” *IEEE Transactions on Neural Networks and Learning Systems*, vol. 35, no. 1, pp. 23–44, 2022.
- [17] L. Shao, F. Zhu, and X. Li, “Transfer learning for visual categorization: A survey,” *IEEE Transactions on Neural Networks and Learning Systems*, vol. 26, no. 5, pp. 1019–1034, 2015.
- [18] J. Yosinski, J. Clune, Y. Bengio, and H. Lipson, “How transferable are features in deep neural networks?” *Advances in neural information processing systems*, vol. 27, 2014.
- [19] S. Chen, L. Han, X. Liu, Z. He, and X. Yang, “Subspace distribution adaptation frameworks for domain adaptation,” *IEEE Transactions on Neural Networks and Learning Systems*, vol. 31, no. 12, pp. 5204–5218, 2020.
- [20] J. Huang, N. Xiao, and L. Zhang, “Balancing transferability and discriminability for unsupervised domain adaptation,” *IEEE Transactions on Neural Networks and Learning Systems*, vol. 35, no. 4, pp. 5807–5814, 2024.
- [21] H. Wang, L. Zheng, H. Zhao, S. Li, and X. Li, “Unsupervised domain adaptation with class-aware memory alignment,” *IEEE Transactions on Neural Networks and Learning Systems*, vol. 35, no. 7, pp. 9930–9942, 2024.
- [22] S. Ma, Z. Yuan, Q. Wu, Y. Huang, X. Hu, C. H. Leung, D. Wang, and Z. Huang, “Deep into the domain shift: Transfer learning through

- dependence regularization,” *IEEE Transactions on Neural Networks and Learning Systems*, vol. 35, no. 10, pp. 14 409–14 423, 2024.
- [23] S. Li, R. Zhang, K. Gong, M. Xie, W. Ma, and G. Gao, “Source-free active domain adaptation via augmentation-based sample query and progressive model adaptation,” *IEEE Transactions on Neural Networks and Learning Systems*, vol. 36, no. 2, pp. 2538–2550, 2025.
- [24] Z. Wen, Q. Li, Y. Wang, H. Shao, and G. Sun, “Fgplfa: Fine-grained pseudo-labeling and feature alignment for source-free unsupervised domain adaptation,” *IEEE Transactions on Neural Networks and Learning Systems*, pp. 1–15, 2025.
- [25] X. Liu, W. Li, and Y. Yuan, “Decoupled unbiased teacher for source-free domain adaptive medical object detection,” *IEEE Transactions on Neural Networks and Learning Systems*, vol. 35, no. 6, pp. 7287–7298, 2024.
- [26] Y. Sun, X. Wang, Z. Liu, J. Miller, A. Efros, and M. Hardt, “Test-time training with self-supervision for generalization under distribution shifts,” in *International Conference on Machine Learning*. PMLR, 2020, pp. 9229–9248.
- [27] Y. Liu, P. Kothari, B. Van Delft, B. Bellot-Gurlet, T. Mordan, and A. Alahi, “Ttt++: When does self-supervised test-time training fail or thrive?” *Advances in Neural Information Processing Systems*, vol. 34, pp. 21 808–21 820, 2021.
- [28] L. Yuan, B. Xie, and S. Li, “Robust test-time adaptation in dynamic scenarios,” in *Proceedings of the IEEE/CVF Conference on Computer Vision and Pattern Recognition*, 2023, pp. 15 922–15 932.
- [29] T. Gong, J. Jeong, T. Kim, Y. Kim, J. Shin, and S.-J. Lee, “Note: Robust continual test-time adaptation against temporal correlation,” *Advances in Neural Information Processing Systems*, vol. 35, pp. 27 253–27 266, 2022.
- [30] B. Zhao, C. Chen, and S.-T. Xia, “Delta: Degradation-free fully test-time adaptation,” in *International Conference on Learning Representations*, 2023.
- [31] D. Tomar, G. Vray, J.-P. Thiran, and B. Bozorgtabar, “Un-mixing test-time normalization statistics: Combatting label temporal correlation,” in *International Conference on Learning Representations*, 2024.
- [32] R. A. Marsden, M. Döbler, and B. Yang, “Universal test-time adaptation through weight ensembling, diversity weighting, and prior correction,” in *Proceedings of the IEEE/CVF Winter Conference on Applications of Computer Vision*, 2024, pp. 2555–2565.
- [33] Z. Zhou, L.-Z. Guo, L.-H. Jia, D. Zhang, and Y.-F. Li, “Ods: Test-time adaptation in the presence of open-world data shift,” in *International Conference on Machine Learning*. PMLR, 2023, pp. 42 574–42 588.
- [34] Z. Nado, S. Padhy, D. Sculley, A. D’Amour, B. Lakshminarayanan, and J. Snoek, “Evaluating prediction-time batch normalization for robustness under covariate shift,” *arXiv preprint arXiv:2006.10963*, 2020.
- [35] P. Bandi, O. Geessink, Q. Manson, M. Van Dijk, M. Balkenhol, M. Hermesen, B. E. Bejnordi, B. Lee, K. Paeng, A. Zhong *et al.*, “From detection of individual metastases to classification of lymph node status at the patient level: the camelyon17 challenge,” *IEEE Transactions on Medical Imaging*, vol. 38, no. 2, pp. 550–560, 2018.
- [36] Y. Zhang, X. Wang, K. Jin, K. Yuan, Z. Zhang, L. Wang, R. Jin, and T. Tan, “Adanpc: Exploring non-parametric classifier for test-time adaptation,” in *International Conference on Machine Learning*. PMLR, 2023, pp. 41 647–41 676.
- [37] A. Karmanov, D. Guan, S. Lu, A. El Saddik, and E. Xing, “Efficient test-time adaptation of vision-language models,” in *Proceedings of the IEEE/CVF Conference on Computer Vision and Pattern Recognition*, 2024, pp. 14 162–14 171.
- [38] C. Wei, K. Shen, Y. Chen, and T. Ma, “Theoretical analysis of self-training with deep networks on unlabeled data,” *International Conference on Learning Representations*, 2021.
- [39] D. Hendrycks and T. G. Dietterich, “Benchmarking neural network robustness to common corruptions and surface variations,” *arXiv preprint arXiv:1807.01697*, 2018.
- [40] K. Saito, D. Kim, S. Sclaroff, T. Darrell, and K. Saenko, “Semi-supervised domain adaptation via minimax entropy,” in *Proceedings of the IEEE/CVF international conference on computer vision*, 2019, pp. 8050–8058.
- [41] M. Döbler, R. A. Marsden, and B. Yang, “Robust mean teacher for continual and gradual test-time adaptation,” in *Proceedings of the IEEE/CVF Conference on Computer Vision and Pattern Recognition*, 2023, pp. 7704–7714.
- [42] F. Croce, M. Andriushchenko, V. Schwag, E. DeBenedetti, N. Flammarion, M. Chiang, P. Mittal, and M. Hein, “Robustbench: a standardized adversarial robustness benchmark,” in *Thirty-fifth Conference on Neural Information Processing Systems Datasets and Benchmarks Track*, 2021. [Online]. Available: <https://openreview.net/forum?id=SSKZPJc7B>
- [43] S. Zagoruyko and N. Komodakis, “Wide residual networks,” *arXiv preprint arXiv:1605.07146*, 2016.
- [44] S. Xie, R. Girshick, P. Dollár, Z. Tu, and K. He, “Aggregated residual transformations for deep neural networks,” in *Proceedings of the IEEE/CVF Conference on Computer Vision and Pattern Recognition*, 2017, pp. 1492–1500.
- [45] D. Hendrycks, N. Mu, E. D. Cubuk, B. Zoph, J. Gilmer, and B. Lakshminarayanan, “Augmix: A simple data processing method to improve robustness and uncertainty,” in *International Conference on Learning Representations*, 2020.
- [46] K. He, X. Zhang, S. Ren, and J. Sun, “Deep residual learning for image recognition,” in *Proceedings of the IEEE/CVF Conference on Computer Vision and Pattern Recognition*, 2016, pp. 770–778.
- [47] G. Huang, Z. Liu, L. Van Der Maaten, and K. Q. Weinberger, “Densely connected convolutional networks,” in *Proceedings of the IEEE conference on computer vision and pattern recognition*, 2017, pp. 4700–4708.
- [48] P. W. Koh, S. Sagawa, H. Marklund, S. M. Xie, M. Zhang, A. Balsubramani, W. Hu, M. Yasunaga, R. L. Phillips, I. Gao *et al.*, “Wilds: A benchmark of in-the-wild distribution shifts,” in *International conference on machine learning*. PMLR, 2021, pp. 5637–5664.
- [49] A. Dosovitskiy, “An image is worth 16x16 words: Transformers for image recognition at scale,” *arXiv preprint arXiv:2010.11929*, 2020.
- [50] H. Wang, X. Wu, Z. Huang, and E. P. Xing, “High-frequency component helps explain the generalization of convolutional neural networks,” in *Proceedings of the IEEE/CVF conference on computer vision and pattern recognition*, 2020, pp. 8684–8694.
- [51] Z. J. Xu, “Understanding training and generalization in deep learning by fourier analysis,” *arXiv preprint arXiv:1808.04295*, 2018.
- [52] Z.-Q. J. Xu, Y. Zhang, and Y. Xiao, “Training behavior of deep neural network in frequency domain,” in *Neural Information Processing: 26th International Conference, ICONIP 2019, Sydney, NSW, Australia, December 12–15, 2019, Proceedings, Part 1* 26. Springer, 2019, pp. 264–274.
- [53] D. Yin, R. Gontijo Lopes, J. Shlens, E. D. Cubuk, and J. Gilmer, “A fourier perspective on model robustness in computer vision,” *Advances in Neural Information Processing Systems*, vol. 32, 2019.
- [54] R. Soklaski, M. Yee, and T. Tsiligkaridis, “Fourier-based augmentations for improved robustness and uncertainty calibration,” in *NeurIPS 2021 Workshop on Distribution Shifts: Connecting Methods and Applications*.
- [55] P. Vaish, S. Wang, and N. Strisciuglio, “Fourier-basis functions to bridge augmentation gap: Rethinking frequency augmentation in image classification,” in *Proceedings of the IEEE/CVF Conference on Computer Vision and Pattern Recognition*, 2024, pp. 17 763–17 772.
- [56] C. Liu, W. Xiang, Y. He, H. Xue, S. Zheng, and H. Su, “Improving model generalization by on-manifold adversarial augmentation in the frequency domain,” *Journal of Visual Communication and Image Representation*, vol. 109, p. 104437, 2025.
- [57] Y. Long, Q. Zhang, B. Zeng, L. Gao, X. Liu, J. Zhang, and J. Song, “Frequency domain model augmentation for adversarial attack,” in *European conference on computer vision*. Springer, 2022, pp. 549–566.
- [58] Y. Yang and S. Soatto, “Fda: Fourier domain adaptation for semantic segmentation,” in *Proceedings of the IEEE/CVF conference on computer vision and pattern recognition*, 2020, pp. 4085–4095.
- [59] C. Yang, X. Guo, Z. Chen, and Y. Yuan, “Source free domain adaptation for medical image segmentation with fourier style mining,” *Medical Image Analysis*, vol. 79, p. 102457, 2022.
- [60] Q. Xu, R. Zhang, Y. Zhang, Y. Wang, and Q. Tian, “A fourier-based framework for domain generalization,” in *Proceedings of the IEEE/CVF conference on computer vision and pattern recognition*, 2021, pp. 14 383–14 392.
- [61] Q. Xu, R. Zhang, Z. Fan, Y. Wang, Y.-Y. Wu, and Y. Zhang, “Fourier-based augmentation with applications to domain generalization,” *Pattern Recognition*, vol. 139, p. 109474, 2023.
- [62] B. Gholami, P. Sahu, O. Rudovic, K. Bousmalis, and V. Pavlovic, “Unsupervised multi-target domain adaptation: An information theoretic approach,” *IEEE Transactions on Image Processing*, vol. 29, pp. 3993–4002, 2020.
- [63] Z. Liu, Z. Miao, X. Pan, X. Zhan, D. Lin, S. X. Yu, and B. Gong, “Open compound domain adaptation,” in *Proceedings of the IEEE/CVF Conference on Computer Vision and Pattern Recognition*, 2020, pp. 12 406–12 415.
- [64] T. Feng, H. Shi, X. Liu, W. Feng, L. Wan, Y. Zhou, and D. Lin, “Open compound domain adaptation with object style compensation

- for semantic segmentation,” *Advances in Neural Information Processing Systems*, vol. 36, 2024.
- [65] K. Hsieh, A. Phanishayee, O. Mutlu, and P. Gibbons, “The non-iid data quagmire of decentralized machine learning,” in *International Conference on Machine Learning*. PMLR, 2020, pp. 4387–4398.
- [66] B. McMahan, E. Moore, D. Ramage, S. Hampson, and B. A. y Arcas, “Communication-efficient learning of deep networks from decentralized data,” in *Artificial intelligence and statistics*. PMLR, 2017, pp. 1273–1282.
- [67] R. McDonald, K. Hall, and G. Mann, “Distributed training strategies for the structured perceptron,” in *Human language technologies: The 2010 annual conference of the North American chapter of the association for computational linguistics*, 2010, pp. 456–464.